Modeling of Photobleaching for the Photoinitiation of Thick Polymerization Systems

G. A. MILLER, L. GOU, V. NARAYANAN, A. B. SCRANTON

Department of Chemical and Biochemical Engineering, University of Iowa, Iowa City, Iowa 52242

Received 4 September 2001; accepted 28 December 2001

ABSTRACT: We present a mathematical description of the spatial and temporal evolution of the light intensity gradient, initiator concentration gradient, and initiation rate profiles for photobleaching initiator systems. This article builds on the foundation provided by previous researchers' contributions by generalizing the governing differential equations to include the effects of absorption by the initiator fragments, absorption by the monomer, and diffusion of the initiator. Simulation results have confirmed that, at any given time, the initiation rate profile resembles a wave front that propagates through the sample. The simulation results suggest that there is an optimum initiator concentration for efficient photopolymerization of thick samples. As either the initiator concentration or molar absorptivity is increased, the initiation rate at the peak of the wave front increases, the breadth of the propagating front decreases, and the rate of spatial propagation through the sample decreases. In contrast, the maximum photoinitiation rate and rate of spatial propagation of the initiation front can be simultaneously increased with an increasing initiator quantum yield or a decreasing absorptivity of the monomer or photolysis products. Finally, on the basis of these studies, diffusion is expected to have negligible effects in most photobleaching systems. © 2002 Wiley Periodicals, Inc. J Polym Sci Part A: Polym Chem 40: 793–808, 2002; DOI 10.1002/pola.10162

Keywords: photopolymerization; computer modeling; radical polymerization

INTRODUCTION

Photopolymerizations are generally chain polymerizations in which propagating active centers (usually radicals or cations) are produced by a light-induced chemical reaction. A wide variety of photoinitiators are available that produce free radicals upon the absorption of photons of the appropriate energy (typically in the ultraviolet or visible regions of the spectrum).[1–3] The photochemical mechanism of active center generation has been well characterized and generally proceeds by α cleavage, β cleavage, or hydrogen abstraction.[4–6] In each of these reactions, the photoinitiator is promoted to an excited state and then fragments (photoscission) or participates in an electron-transfer reaction to produce active centers.

Photopolymerization has emerged as an inexpensive and efficient method for producing polymeric films and coatings with reduced emissions of volatile organic components. Light-induced polymerization offers a number of advantages over the thermal curing of polymers, including spatial and temporal control of the initiation, high reaction rates, and lower energy requirements, which are important factors for a wide range of applications.[7–9] Although radiation curing first gained prominence as a rapid and efficient method for producing films and coatings, recently, photocuring has found applications in the production of thick polymers and composites.[10–13] To effectively cure a thick section, the initiator system and

Correspondence to: A. B. Scranton (E-mail: abscran@engineering.uiowa.edu)

Journal of Polymer Science: Part A: Polymer Chemistry, Vol. 40, 793–808 (2002)
© 2002 Wiley Periodicals, Inc.

wavelength must be carefully selected to ensure that light can effectively penetrate the sample. Ideally, the initiation wavelength should be selected so that the initiator is the only absorbing species (the monomer or such should be nonabsorbing). In addition, for a thick-section cure, it is often desirable to have a lower initiator concentration and/or extinction coefficient than for the photocuring of thin films. Finally, a number of investigators have found that it is advantageous to use photobleaching initiators in which light absorption by the initiator products is lower than that by the original photoinitiator molecule, thereby allowing more light to pass through the system.

A number of initiators exhibit photobleaching characteristics. For example, the photolysis products of benzoin ethyl ether (BEE), when irradiated with ultraviolet light in a solution of deoxygenated benzene, are benzil, benzaldehyde, and picanol ethers.[14] These molecules are considerably less absorbing at 365 nm than BEE itself; therefore, photobleaching is observed upon irradiation of a solution of BEE at 365 nm. Photobleaching is particularly pronounced in solutions of acyl and bisacyl phosphine oxides because photolysis results in cleavage of the carbon phosphorus bond, thereby destroying the chromophore that absorbs in the near ultraviolet–visible region (350–410 nm). Substituted titanocenes are another class of photoinitiators that have excellent bleaching properties in the 440-nm region.[15]

In a photobleaching system, the light intensity gradient in the sample depends on both the time and depth beneath the illuminated surface. Initially, the initiator concentration is uniform, and the light intensity will decrease exponentially with depth, as described by Beer's law. Immediately after illumination, the initiator will be consumed at a rate proportional to the local light intensity, thereby leading to an initiator concentration gradient with the lowest concentration on the exposed surface. A mathematical description of photoinitiation in a photobleaching system is complicated by the fact that the light intensity gradient and the initiator concentration gradient are coupled in this way. As recently described by Terrones and Pearlstein,[16] previous attempts to account for the variations of light intensity and initiation rate have failed to accurately describe these complex systems. Recently, two research groups[16,17] provided theoretical descriptions of initiation in photobleaching systems for the case in which only the original photoinitiator molecule absorbs (the monomer and initiator fragments were assumed to be nonabsorbing at the initiation wavelength).

Terrones and Pearlstein[16] provided an excellent account of the shortcomings of the previous descriptions of photoinitiation, which did not correctly account for the effects of the spatial variation of the initiation rate. These authors presented an unsteady-state, one-dimensional model that properly accounted for the initiator consumption and optical attenuation for free-radical photopolymerizations in photobleaching systems. Through an examination of the case in which only the photoinitiator absorbed at the initiating wavelength, the resulting integro-differential equation could be solved analytically. These authors also effectively assumed that the sample was illuminated with monochromatic light (the absorption of light is described with a single absorption coefficient) and that mixing by diffusion or convection was negligible. Terrones and Pearlstein presented results for the variations of the photoinitiator concentration and the photoinitiation rate as functions of sample depth for systems with an initial absorbance γ (the product of the initiator absorption coefficient, initial initiator concentration, and sample thickness) ranging from 0.1 to 100. Interestingly, the authors found that with increasing initial absorbance, the local initiation rate becomes increasingly nonuniform and, for high γ, assumes the form of a localized wave that propagates through the sample.

In a recent contribution, Ivanov and Decker[17] also discussed the inherent inability of the standard theoretical treatments of photopolymerization kinetics to account for the spatial variation of the initiation rate. These authors solved the coupled differential equations that describe the spatial and temporal evolution of both the light intensity gradient and the initiator concentration gradient. Again, because the initiator fragments and the monomer were both assumed to be nonabsorbing, the equations could be solved analytically. The authors assumed that initiation was by monochromatic light, and diffusion was neglected. The initiation kinetics were coupled to the polymerization kinetics with a quasi-steady-state approximation for bimolecular radical termination. Ivanov and Decker demonstrated that, under these assumptions, the light intensity gradients in the sample depended primarily on the absorption coefficient and initial concentration of the initiator. The influence of sample thickness on the kinetics of the photoinitiator and monomer consumption was investigated for systems vary-

ing from transparent films to optically thick samples.

In this article, we present a more generalized description of the spatial and temporal evolution of the light intensity gradient and the initiator concentration gradient in photobleaching systems. This article builds on the foundation provided by Terrones and Pearlstein[16] and Ivanov and Decker[17] by generalizing the governing differential equations to include the effects of absorption by the initiator fragments, absorption by the monomer, and diffusion of the initiator. Because of the complexity of the resulting set of coupled differential equations, a numerical solution was obtained with the method of finite differences. The simulation results illustrate the effects of a variety of system variables on the time evolution of the initiator concentration gradient, the light intensity gradient, and, ultimately, the photoinitiation rate profiles.

GENERALIZED GOVERNING DIFFERENTIAL EQUATIONS

For an initially homogeneous sample subject to uniform illumination normal to the surface, the evolution of the light intensity gradient through the depth of the sample is dependent on the concentration of initiator, which also varies with sample depth and time. For the generalized case, which includes the effects of absorption by the initiator fragments, absorption by the monomer, and initiator diffusion, the following set of coupled partial differential equations describes the light intensity and initiator concentration profiles:

$$\frac{\partial C_i(z,t)}{\partial t} = -\varepsilon_i \phi_i \left(\frac{I(z,t)}{N_A h \nu}\right) C_i(z,t) + D_i \frac{\partial^2 C_i(z,t)}{\partial z^2} \quad (1)$$

$$\frac{\partial C_p(z,t)}{\partial t} = \varepsilon_i \phi_i \left(\frac{I(z,t)}{N_A h \nu}\right) C_i(z,t) + D_p \frac{\partial^2 C_p(z,t)}{\partial z^2} \quad (2)$$

$$\frac{\partial I(z,t)}{\partial z} = -[\varepsilon_i C_i(z,t) + A_m + \varepsilon_p C_p(z,t)] I(z,t) \quad (3)$$

where $C_i(z,t)$ represents the initiator molar concentration at depth z and time t; $C_p(z,t)$ represents the photolysis product molar concentration at depth z and time t; $I(z,t)$ represents the incident light intensity at depth z and time t, with dimensions of energy/(area $\times$ time); ϵ_i is the initiator molar absorptivity with dimensions of volume/(length $\times$ mole); ϵ_p is the photolysis product molar absorptivity, with dimensions of volume/(length $\times$ mole), and accounts for the photon absorption by all fragmentation species; N_A is Avogadro's number; h is Planck's constant; υ is the frequency of light, with dimensions of inverse time; ϕ_i is the quantum yield of the initiator, defined as the fraction of absorbed photons that lead to fragmentation of the initiator; D_i is the diffusion coefficient for the initiator, with dimensions of length^2/time; D_p is the diffusion coefficient for the photolysis products; and A_m is the absorption coefficient of the monomer and the polymer repeat unit (the product of the molar absorptivity and the molar concentration of the monomer units), with dimensions of inverse length.

In these governing equations, division of the incident light intensity $I(z,t)$ by the product $N_A h\upsilon$ simply converts the intensity into the photon flux, with dimensions of moles of photons per unit of area per unit of time. Note that in eq 1, the change in initiator concentration with time includes one contribution from the consumption of initiator in the photochemical reaction and a second from the diffusion of the initiator that arises from the resulting concentration gradient. Equation 2, which describes the initiator products (fragments), has one contribution accounting for the production of the fragments in the photochemical reaction and a second for diffusion. Finally, the light intensity profile through the depth of the sample is represented in eq 3 and includes terms arising from the absorbance by the initiator, monomer, and photolysis products. Note that any change in the monomer absorption coefficient upon polymerization has been neglected in the development of the governing differential equations.

The following boundary conditions and initial conditions apply to this system:

$$C_i(z,0) = C_0 \quad (4)$$

$$C_p(z,0) = 0 \quad (5)$$

$$\frac{dC_{i,p}}{dz} = 0 \text{ at } z = 0 \text{ and}$$

$$z = z_{max} \text{ (the thickness of the sample)} \quad (6)$$

$$I(0,t) = I_0 \quad (7)$$

Equation 4 accounts for the fact that the initiator concentration is initially uniform through

the depth of the sample. Equation 5 indicates that photolysis product concentration is initially equal to zero throughout the sample, whereas eq 6 represents the no-flux boundary condition at the ends of the sample for both the initiator and the fragments (this boundary condition is necessary because of the diffusional terms in the governing equations). Finally, eq 7 indicates that the light intensity at the exposed surface is equal to the incident light intensity at all times.

The simplification of eqs 1–3 by the elimination of the diffusion term and the setting of the absorption coefficients of the monomer and photolysis products to zero leads to the following equations:

$$\frac{\partial C_i(z,t)}{\partial t} = -\varepsilon_i \phi_i \left(\frac{I(z,t)}{N_A h\nu}\right) C_i(z,t) \tag{8}$$

$$\frac{\partial I(z,t)}{\partial z} = -\varepsilon_i C_i(z,t) I(z,t) \tag{9}$$

This simplified set of equations is equivalent to eqs 3 and 4 in the article by Ivanov and Decker[17] and eq 9a in the article by Terrones and Pearlstein.[16]

RESULTS AND DISCUSSION

In the remainder of this article, eqs 1–7 are solved simultaneously to illustrate the effects of a variety of system variables on the time evolution of the initiator concentration gradient, the light intensity gradient, and, ultimately, the photoinitiation rate profiles. The simulation conditions are selected to illustrate the effects of the concentration, molar absorptivity, and quantum yield of the initiator, the absorptivity of the initiator fragments and the monomer, and the effect of diffusion, with the goal of identifying selection criteria for the effective photopolymerization of thick systems. In future contributions, the effect of multiple wavelength initiation will be investigated.

Representative Simulation Results

The governing differential equations (eqs 1–7) were solved numerically with the method of finite differences to obtain profiles of the light intensity, initiator concentration, and initiation rates as functions of time and depth. For accurate results, a finite difference mesh size of about 1 s in the time domain and 0.025 cm in the depth domain was used. To verify the accuracy of the numerical method, we compared the numerical solution to the analytical solution reported by Terrones and Pearlstein[16] for the case of no diffusion and no absorption by the initiator fragments and monomer. The two models gave essentially identical results at time zero, and any deviation would increase with illumination time. Therefore, the comparison of this model with the analytical solution of Terrones and Pearlstein[16] was made late in the reaction when more than 90% of the photoinitiator had been consumed. For the mesh sizes listed, the correlation of fit (R^2) for a comparison of the initiator concentration profiles was greater than 0.994 under these stringent test conditions. This result confirms the accuracy of the numerical solution.

Representative simulation results for a sample with a relatively low optical density are shown in Figures 1 and 2. These results would arise from a molar concentration of 0.0268 mol/L for an initiator with a molar extinction coefficient of 97.7 L cm^{-1} mol^{-1}. Figure 1 contains a plot of the normalized initiator concentration [defined as $C(z,t)/C_0$] as a function of sample depth in centimeters for a system with no absorption by the monomer or the initiator fragments and no initiator diffusion. This serves as a base case to which more complex systems can be compared. The plot illustrates that at time $t = 0$, the initiator concentration is independent of depth with a uniform normalized concentration of unity. Correspondingly, as shown in Figure 2, the light intensity initially decreases exponentially in accordance with Beer's law. As time passes, the initiator is consumed at a rate proportional to the local light intensity, causing the concentration to decrease the fastest at locations near the illuminated surface. This results in an increased transmittance of light near the surface, further increasing the rate of consumption of the initiator. The effects of this bleaching process on the initiator concentration and the light intensity is illustrated by the family of curves in Figures 1 and 2. For example, note that the initiator concentration assumes a sigmoidal shape with nearly zero concentration near the illuminated surface in Figure 1. With time, the region with nearly zero initiator concentration (and nearly 100% transmittance of light) expands as the system bleaches. For this set of simulation conditions, the transmittance of the sample reaches a normalized value of 0.9 in 64 s and a normalized value of 0.99 in 81 s. This relatively fast bleaching results from the relatively high light intensity, the relatively low initiator concen-

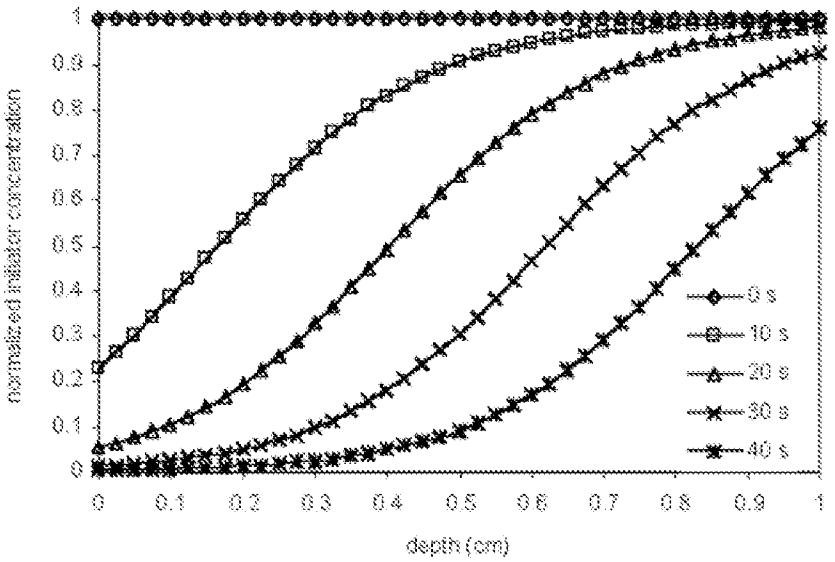

Figure 1. Time and depth dependence of the initiator concentration in a 1.0-cm sample. The light intensity is 10 mW/mm^2, C_0 is 0.0268 M (0.4 wt %), ϕ is 0.2, ϵ_i is 97.7 L (mol cm)$^{-1}$, and ϵ_p is 0 L (mol cm)$^{-1}$. Mesh sizes are 1.0 s and 0.025 cm.

tration, the high initiator molar absorptivity, and the lack of absorption by the monomer and the initiator fragments. As illustrated in the next few sections, the initiator concentration and molar absorptivity both play important roles in determining the rate of photobleaching and, therefore, the effectiveness of the system for thick-section cure.

Effect of the Initiator Concentration

The initiator concentration plays a key role in determining the time evolution of the light intensity gradient in a photobleaching system and, therefore, in the effectiveness of the photopolymerization of thick systems. A number of investigators have identified the importance of the ini-

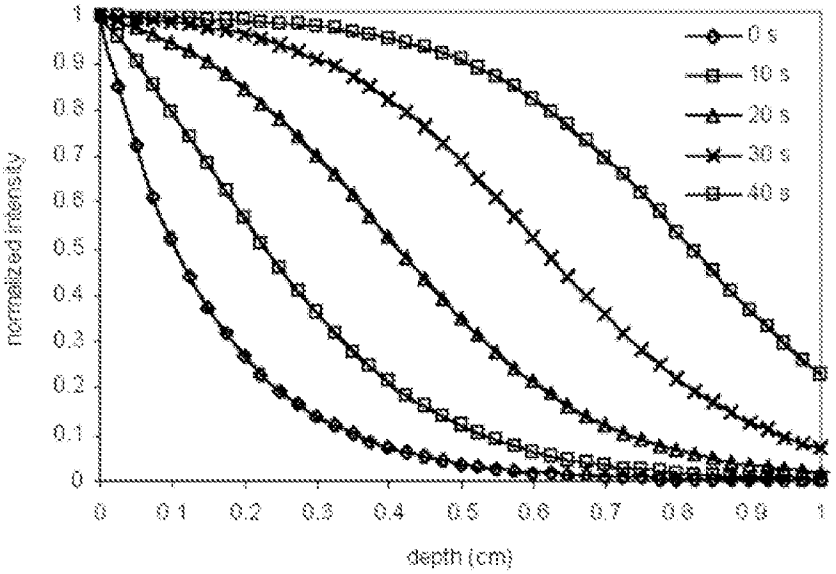

Figure 2. Time and depth dependence of the normalized light intensity in a 1.0-cm sample. The light intensity is 10 mW/mm^2, C_0 is 0.0268 M (0.4 wt %), ϕ is 0.2, ϵ_i is 97.7 L (mol cm)$^{-1}$, and ϵ_p is 0 L (mol cm)$^{-1}$. Mesh sizes are 1.0 s and 0.025 cm.

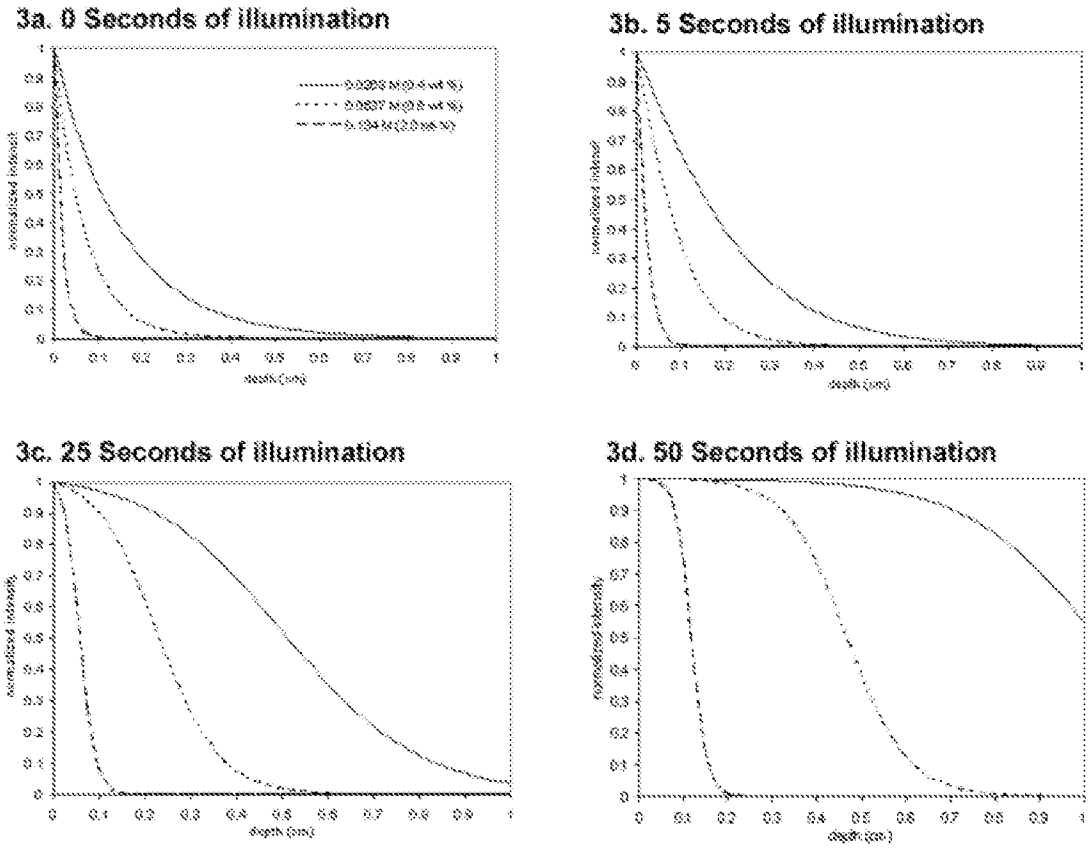

Figure 3. Effect of the various initiator concentrations on the intensity profile in a 1.0-cm sample. The light intensity is 10 mW/mm^2, ϕ is 0.2, ϵ_i is 97.7 L (mol cm)$^{-1}$, and ϵ_p is 0 L (mol cm)$^{-1}$. Mesh sizes are 1.0 s and 0.025 cm.

tiator concentration[10–12,17] and have found that for thick-section cure it is necessary to use lower initiator concentrations than typically used for the photopolymerization of films and coatings. Figure 3 (a–d) illustrates the effect of the initial initiator concentration on the evolution of the light intensity gradient in a photobleaching sample. This figure includes light intensity profiles for three different initial initiator concentrations at four different times, with all other simulation parameters being equal. Figure 3 (a) illustrates that, as expected, at time $t = 0$ (immediately after illumination when the initiator concentration is still uniform), the light intensity decreases exponentially with a depth of penetration that decreases with increasing concentration. Figure 3 (b–d) shows the light intensity gradients for the three initial initiator concentrations at illumination times of 5, 25, and 50 seconds, respectively. These profiles illustrate that the photobleaching process is more rapid and more efficient for the lowest initial initiator concentration and that the differences in the light transmittance among the three systems increases with increasing time. For example, after 50 s of illumination, the systems with initial initiator concentrations of 0.0268, 0.0537, and 0.134 M exhibit a normalized intensity of 90% at depths of 0.700, 0.325, and 0.075 cm, respectively. This effect would be even greater if the molar absorptivity of the initiator fragments were non-zero.

Figure 4 (a–c) illustrates the effect of the initiator concentration on the profiles of the initiation rate as a function of depth. If two active centers are produced upon fragmentation of the initiator, the instantaneous local rate of production of free radicals, $R_i(z,t)$, is represented by the following equation:[16]

$$R_i(z,t) = 2\phi\epsilon_i C_i(z,t) I(z,t) \tag{10}$$

With this equation, the photoinitiation rate $R_i(z,t)$ may be calculated directly from $C_i(z,t)$ and $I(z,t)$ profiles obtained by the numerical solution

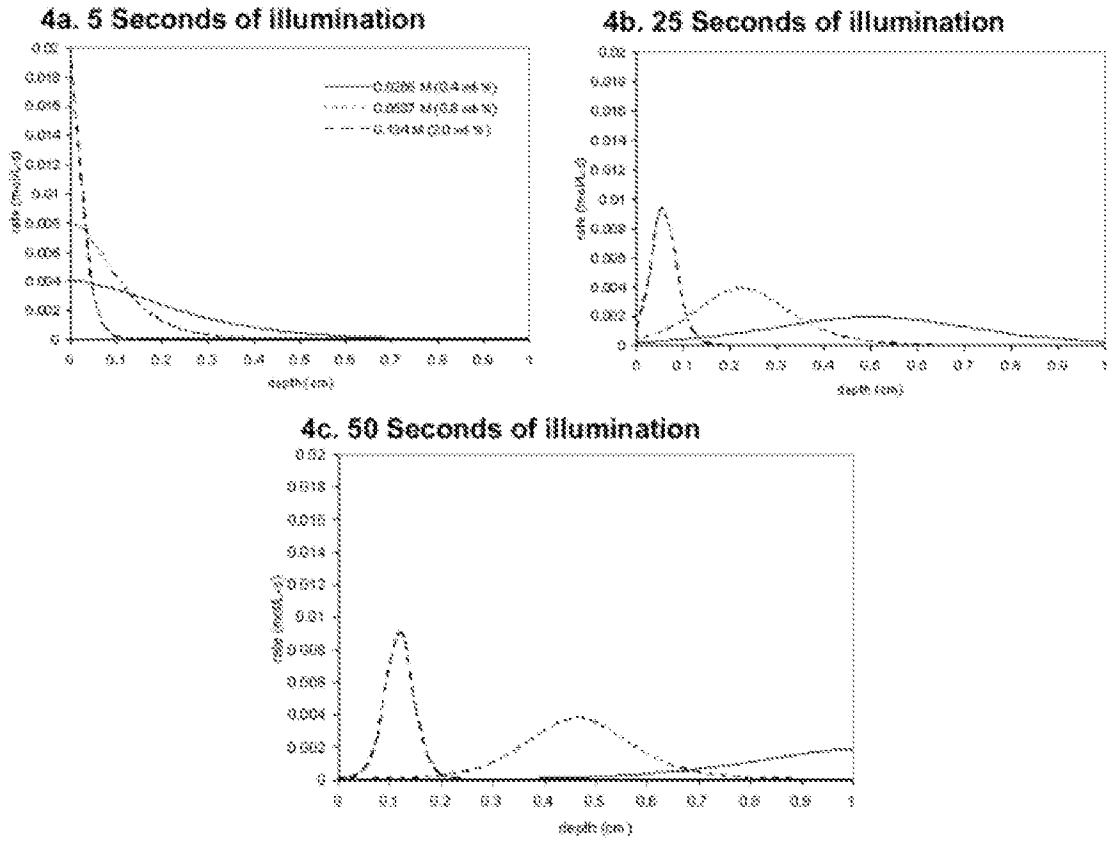

Figure 4. Effect of the various initiator concentrations on the photoinitiation rate in a 1.0-cm sample. The light intensity is 10 mW/mm^2, ϕ is 0.2, ϵ_i is 97.7 L (mol cm)$^{-1}$, and ϵ_p is 0 L (mol cm)$^{-1}$. Mesh sizes are 1.0 s and 0.025 cm.

of eqs 1–7. Figure 4 (a–c) contains profiles of the photoinitiation rate as a function of depth for the same conditions shown previously in Figure 3. An examination of Figure 4 illustrates some interesting trends. In general, the photoinitiation rate is not uniform; rather, it varies significantly with time and depth in the sample. After the initial illumination, the photoinitiation rate profile exhibits a characteristic shape determined by the spatial variation in the product of the light intensity and the initiator concentration. At a given time, with progression through the depth of the sample from the illuminated surface, the initiation rate increases with increasing depth to a maximum rate (for depths smaller than this maximum, the rate is low because the initiator has been depleted in this region) and then decreases with increasing depth because of the reduction in light intensity. As a result, at any given time, the initiation rate profile resembles a wave front, and the breadth of this front is determined by factors such as the initial initiator concentration and the molar absorptivity (the breadth increases with decreasing initial initiator concentration and decreasing molar absorptivity). This type of wave-like propagation through the sample was recently described by Terrones and Pearlstein[16] and Ivanov and Decker.[17]

An examination of Figure 4 (a–c) illustrates some trends that are important for the efficient photopolymerization of thick systems. For example, although the maximum initiation rate is highest for the sample with the highest initiator concentration, the depth of light penetration and the spatial propagation of the photoinitiation front are restricted. In contrast, although low initiation concentrations allow efficient penetration of light into the sample, the photoinitiation rate at a given location is generally low because the rate is limited by the lack of initiator. These results suggest that an intermediate optimum initiator concentration exists for efficient photopolymerization of thick samples in a timely manner.

Effect of the Molar Absorptivity of the Initiator

The molar absorptivity of the initiator also plays an important role in determining the time evolu-

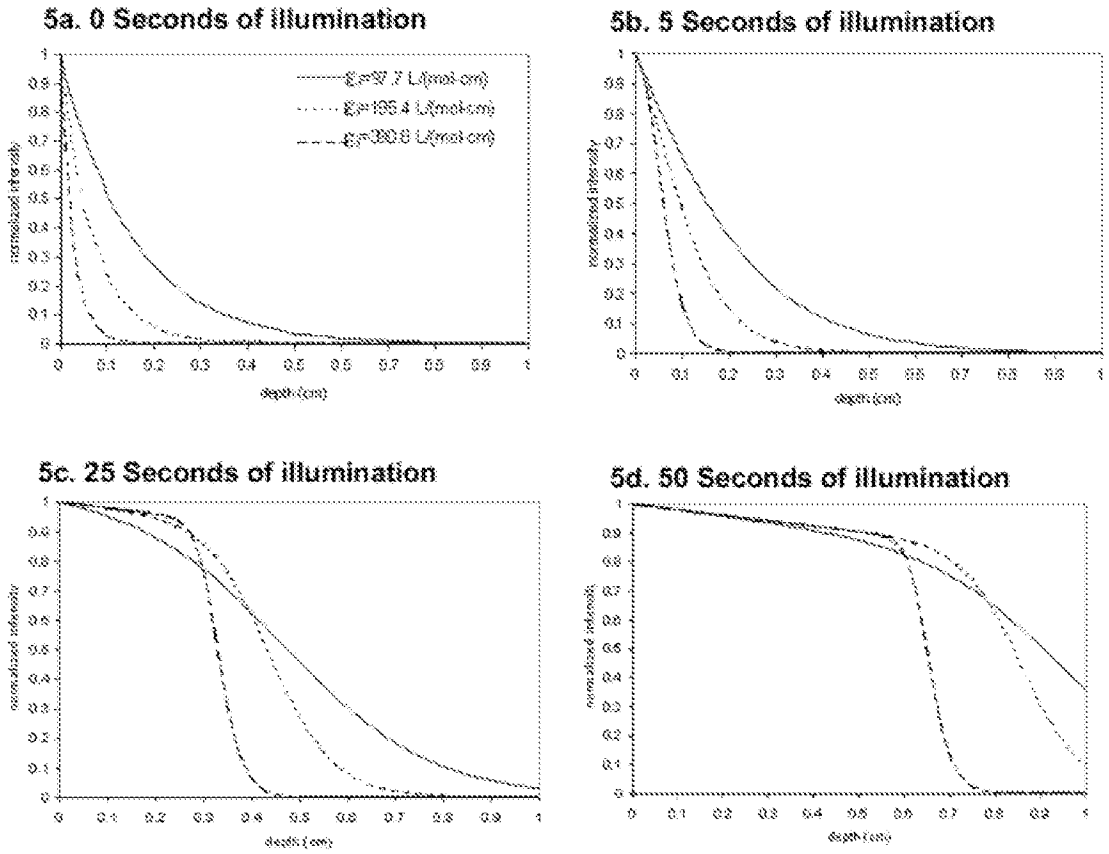

Figure 5. Effect of the initiator absorptivity on the intensity profile of a 1.0-cm sample. The light intensity is 10 mW/mm^2, C_0 is 0.0268 M (0.4 wt %), ϕ is 0.2, and ϵ_p is 0 L (mol cm)$^{-1}$. Mesh sizes are 1.0 s and 0.025 cm

tion of the light intensity gradient in photobleaching systems. Figure 5 (a–d) contains light intensity profiles for three different initiator molar absorptivities at four different times, with all other simulation parameters being equal. Figure 5 (a) illustrates that, as expected, at illumination times near zero [Fig. 5 (a,b)], the light intensity decreases exponentially with a depth of penetration that decreases with increasing initiator absorptivity, and the intensity at every point increases with decreasing molar absorptivity. With increasing illumination time [Fig. 5 (c,d)], the systems with higher initiator absorptivity exhibit higher intensity near the illuminated surface due to consumption of the initiator and the associated photobleaching. This effect arises from the fact that the absorbance of a photon is the first step in the bleaching process, and the system with the higher initiator absorptivity has a higher rate of photon absorption near the illuminated surface. Therefore, Figure 5 illustrates that the initiator absorptivity has two competing effects on the photoinitiation effectiveness for deep cure. A low molar absorptivity allows more efficient penetration of the light into the sample; however, a higher molar absorptivity leads to higher rates of photon absorption and higher rates of bleaching. From these results, it is difficult to identify the optimum initiator absorptivity.

For further investigation of the importance of the initiator absorptivity on the effectiveness of the photopolymerization system, it is instructive to examine profiles of the initiation rate as a function of thickness. Figure 6 illustrates the effect of the initiator molar absorptivity on the photoinitiation rate as a function of depth for the same conditions shown in Figure 5. Figure 6 (a–c) shows that as the initiator molar absorptivity increases, the maximum initiation rate increases, the breadth of the propagating front decreases, and the rate of spatial propagation through the sample decreases. Figure 6 illustrates more clearly that the advantage of the system with the relatively high initiator absorptivity is a locally high rate of initiation that will lead to a higher local rate of polymerization, beginning on the sur-

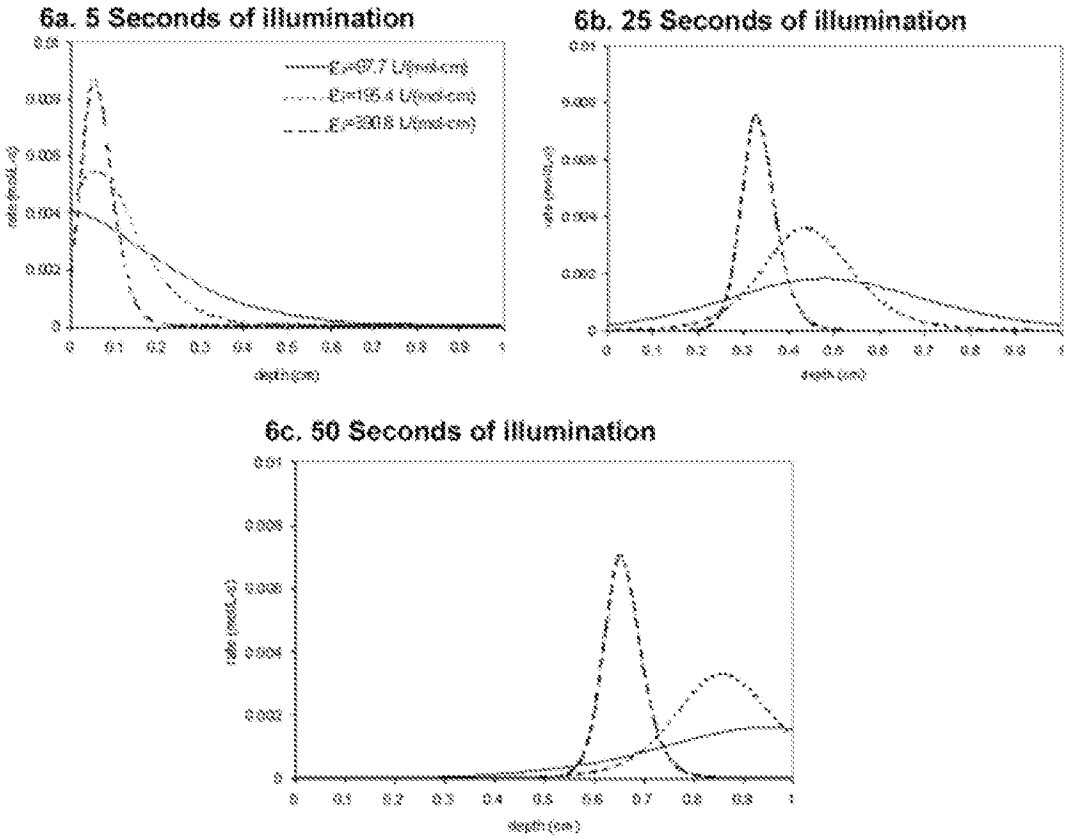

Figure 6. Effect of the initiator absorptivity on the photoinitiation rate of a 1.0-cm sample. The light intensity is 10 mW/mm^2, C_0 is 0.0268 M (0.4 wt %), ϕ is 0.2, and ϵ_p is 0 L (mol cm)$^{-1}$. Mesh sizes are 1.0 s and 0.025 cm.

face. This could allow a barrier polymer to form on the surface, whereas the relatively sharp initiation front moves through the depth of the sample. The advantage of the system with the low absorptivity results from the more efficient light penetration into the sample. These systems exhibit appreciable photoinitiation rates deep into the sample in a relatively short period of time. This result is important for systems that require the development of polymer properties soon after illumination. An initiation system exhibiting both of these advantages could be achieved with two different incident initiation wavelengths with one or more initiators.

Figures 3–6 illustrate the importance of examining the effects of the initiator concentration and absorptivity separately. Because the product of the initial initiator concentration and the initiator absorptivity is proportional to the initial optical density, it is tempting to characterize these two parameters with a single parameter. However, it is important to optimize these two parameters separately because each has distinct effects on the time evolution of the light intensity gradient and the initiation rate profile. For example, consider two systems of equal thickness with the same optical density: one with a high initial initiator concentration and a low absorptivity and the second with a low initial initiator concentration and a high absorptivity. Immediately upon illumination, the two systems will exhibit identical light intensity profiles throughout the sample because the initial optical densities are the same. With increasing time, however, the initiator concentration will change because of photobleaching, whereas the absorptivity remains constant. The system with the higher initiator absorptivity will photobleach more rapidly because a higher fraction of the molecules absorb photons, and the photoinitiation front will propagate more rapidly through the thickness of the sample.

Effect of the Initiator Quantum Yield

It is interesting to contrast the effect of the initiator quantum yield with the effect of the initiator molar

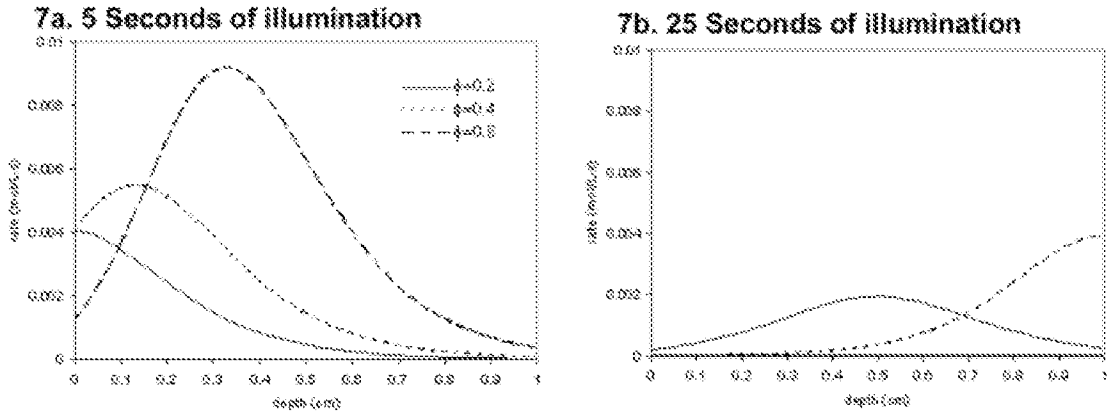

Figure 7. Effect of the initiator quantum yield on the photoinitiation rate of a 1.0-cm sample. The light intensity is 10 mW/mm^2, C_0 is 0.0268 M (0.4 wt %), ϵ_i is 97.7 L (mol cm)$^{-1}$, and ϵ_p is 0 L (mol cm)$^{-1}$. Mesh sizes are 1.0 s and 0.025 cm.

absorptivity discussed previously. Although the molar absorptivity characterizes the probability that the initiator will absorb an incident photon, the quantum yield describes what happens after the photon is absorbed. We assume that the initiator molecules that are not dissociated after absorption will return to the ground state by either radiative or nonradiative processes and will be available for further photochemical reactions (the recent articles by Terrones and Pearlstein[16] and by Ivanov and Decker[17] are based on the same assumption). Figure 7 (a,b) illustrates the effect of the initiator quantum yield on the photoinitiation rate as a function of sample depth. The figure illustrates that as the quantum yield increases from 0.2 to 0.4 and finally to 0.8 with all other simulation variables held constant, the maximum photoinitiation rate increases and the rate of spatial propagation of the polymerization front increases. This is in contrast to the effects of both the initial initiator concentration and the initiator absorptivity. For both of those variables, an increase in the maximum photoinitiation rate had an associated decrease in the rate of propagation of the photoinitiation front.

Effect of the Photolysis Product Absorptivity

The effect of the photolysis product absorptivity on the time evolution of the light intensity gradients is illustrated in Figure 8 (a–d). This figure contains light intensity profiles at four different times for three different molar absorptivities of the photolysis products: $\epsilon_p = 0$, which corresponds to perfect bleaching; $\epsilon_p = 6.5$ L/(mol cm), which corresponds to an intermediate level of bleaching, and $\epsilon_p = 97.7$ L/(mol cm), which is the same absorptivity as the original initiator and, therefore, corresponds to a completely nonbleaching system. Immediately upon illumination, the three systems exhibit identical light intensity profiles because there are no photolysis products at time zero. With increasing time, the light intensity gradient for the system without bleaching remains unchanged, whereas the photobleaching systems allow more efficient light penetration into the sample. Figure 9 (a–c) illustrates the effect of the photolysis product molar absorptivity on the photoinitiation rate profile for the same conditions shown in Figure 8. Figure 9 illustrates that for the nonbleaching system, because the light intensity gradient is stagnant, the photoinitiation rate remains close to zero at the unilluminated end of the sample, and the photoinitiation rate at a given point decreases with time as the photoinitiator is consumed. Therefore, it is difficult to achieve thick-section cure for a nonbleaching photoinitiator, and this effect is magnified for systems as the initiator concentration or sample thickness is increased. Figure 9 illustrates that as the molar absorptivity of the photolysis products is reduced, the rate of propagation of the photoinitiation front increases, and for the perfectly bleaching case, the peak in the photoinitiation rate reaches the bottom of the sample within 50 s for the conditions in the simulation. This time could be reduced further with decreasing initiator concentration or increasing incident light intensity. Again, these results illustrate the importance of proper system design for the efficient photopolymerization of thick systems.

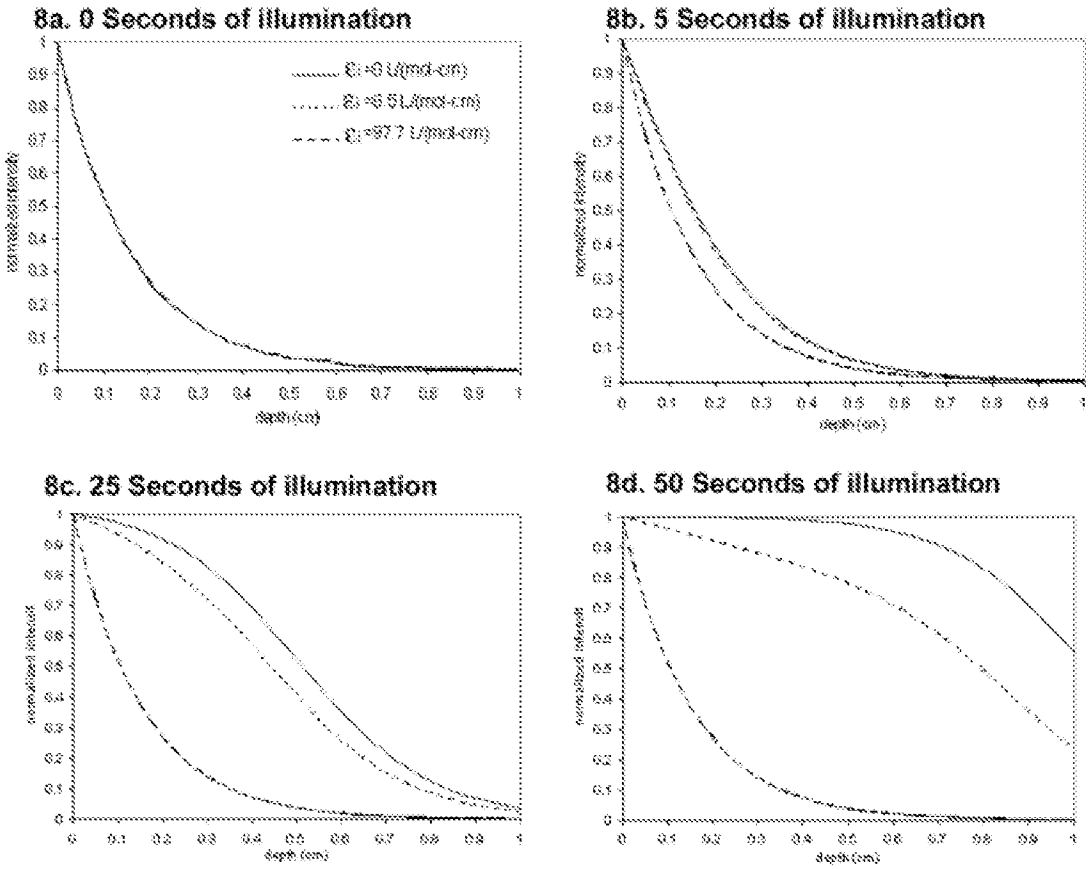

Figure 8. Effect of the photolysis product absorptivity on the intensity profile of a 1.0-cm sample. The light intensity is 10 mW/mm^2, C_0 is 0.0268 M (0.4 wt %), ϕ is 0.2, and ϵ_i is 97.7 L (mol cm)$^{-1}$. Mesh sizes are 1.0 s and 0.025 cm.

Effect of the Monomer Absorption Coefficient

The effect of the monomer absorption coefficient on the time evolution of the light intensity gradients is illustrated in Figure 10 (a–d). This figure contains light intensity profiles at four different times for three different absorption coefficients of the monomer/polymer. For convenience, the absorption coefficient (which is a product of the molar absorptivity and the molar concentration) was chosen to characterize the tendency of the monomer/polymer to absorb photons. Even if the molar absorptivity of the monomer is very low, the absorption coefficient of the monomer may be significant because the monomer molar concentration is generally orders of magnitude higher than that of the initiator. Again, any change in the absorption coefficient upon polymerization has been neglected in the development of the governing differential equations.

For the construction of Figure 10, three representative values of the monomer absorption coefficient have been selected: $A_m = 0$ cm^{-1}, which corresponds to a transparent matrix; $A_m = 0.3$ cm^{-1}; and $A_m = 6$ cm^{-1}. The latter value corresponds to the case in which the monomer absorption coefficient matches that of the initiator at time zero. This figure clearly illustrates the importance of selecting an initiation wavelength for which the monomer is transparent. Although the two systems with relatively low absorption by the monomer allow the light to penetrate the sample with increasing illumination time, the system with the high monomer absorption coefficient has a relatively stagnant light intensity gradient. The effect of monomer absorption on the photoinitiation rate profile is shown in Figure 11. The system with high absorption of light by the monomer exhibits both a lower maximum initiation rate and a relatively stagnant photoinitiation front that reaches only 20% of the sample in the time it takes for the other systems to propagate completely through the depth of the sample. Figure 11 makes it clear that the absorption of light by the monomer/polymer makes much less efficient

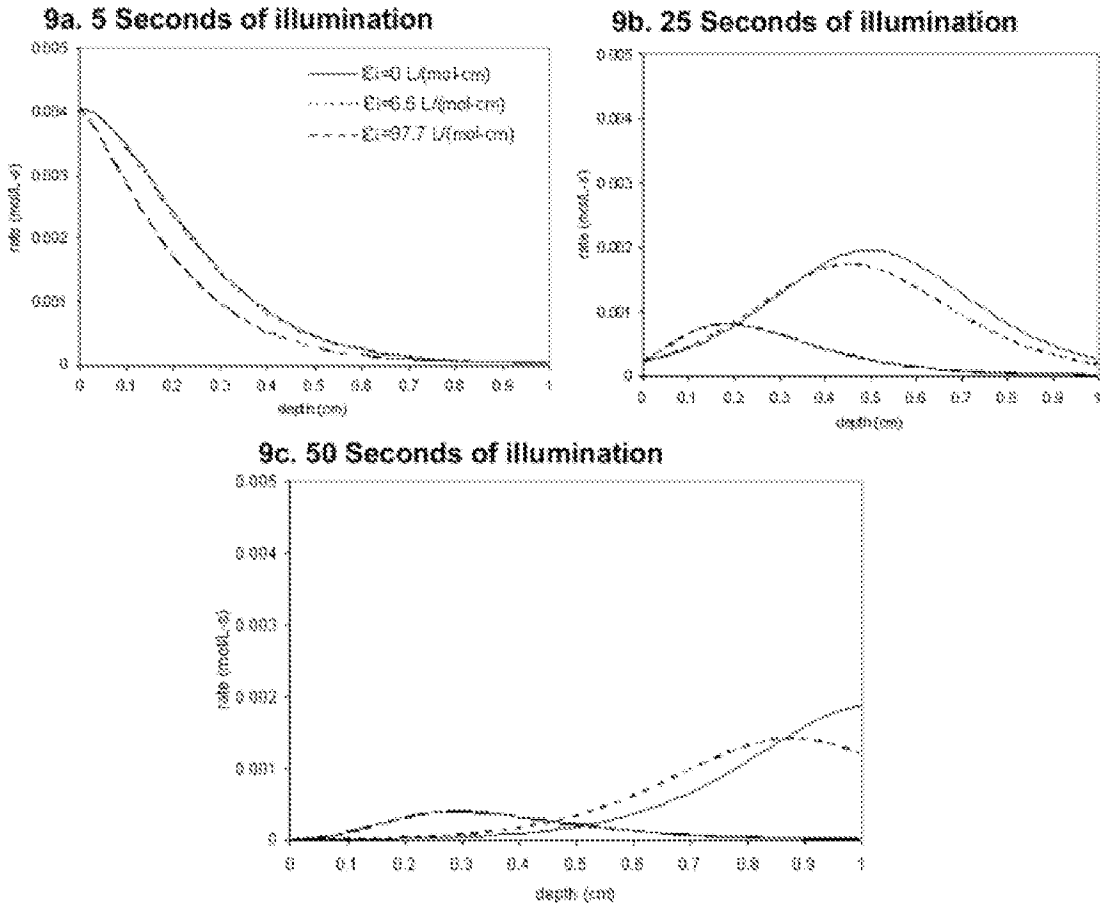

Figure 9. Effect of the photolysis product absorptivity on the photoinitiation rate of a 1.0-cm sample. The light intensity is 10 mW/mm^2, C_0 is 0.0268 M (0.4 wt %), ϕ is 0.2, and ϵ_i is 97.7 L (mol cm)$^{-1}$. Mesh sizes are 1.0 s and 0.025 cm.

use of the incident photons because the integral of the photoinitiation rate profile is greatly reduced. Therefore, by selecting an initiation wavelength that the monomer does not absorb, we can significantly increase the maximum photoinitiation rate (indeed, it is possible to increase the photoinitiation rate throughout the sample) and increase the rate of spatial propagation of the polymerization front. All of these factors lead to more efficient photopolymerization of thick systems.

Effect of the Initiator Diffusion

Diffusion of the unreacted initiator and the photolysis products could arise from the concentration gradients produced in the photobleaching process. The relative importance of diffusion will depend on the value of the diffusion coefficient, the concentration gradient, and the time required for photobleaching to be complete. Diffusion will be more important for photobleaching systems containing high initiator concentrations, which lead to steep concentration gradients and relatively long times for photobleaching. To explore the importance of diffusion in a typical thick-section cure, we have examined the two limiting cases of no diffusion and perfect mixing (which corresponds to an infinitely large diffusion coefficient). Figure 12 contains a plot of the normalized initiator concentration as a function of depth for a representative photobleaching system after 25 s of illumination. The figure contains three curves: one for perfect mixing (which is a horizontal line because the concentration is uniform in this case), one for a representative diffusion coefficient of 0.001 cm^2/s (we chose a relatively large value of the diffusion coefficient to exaggerate the diffusional effects), and a third corresponding to the lack of diffusion. Similarly, Figure 13 contains a plot of the light intensity as a function of the sample depth for the same system shown in Figure 12. The system corresponding to perfect mix-

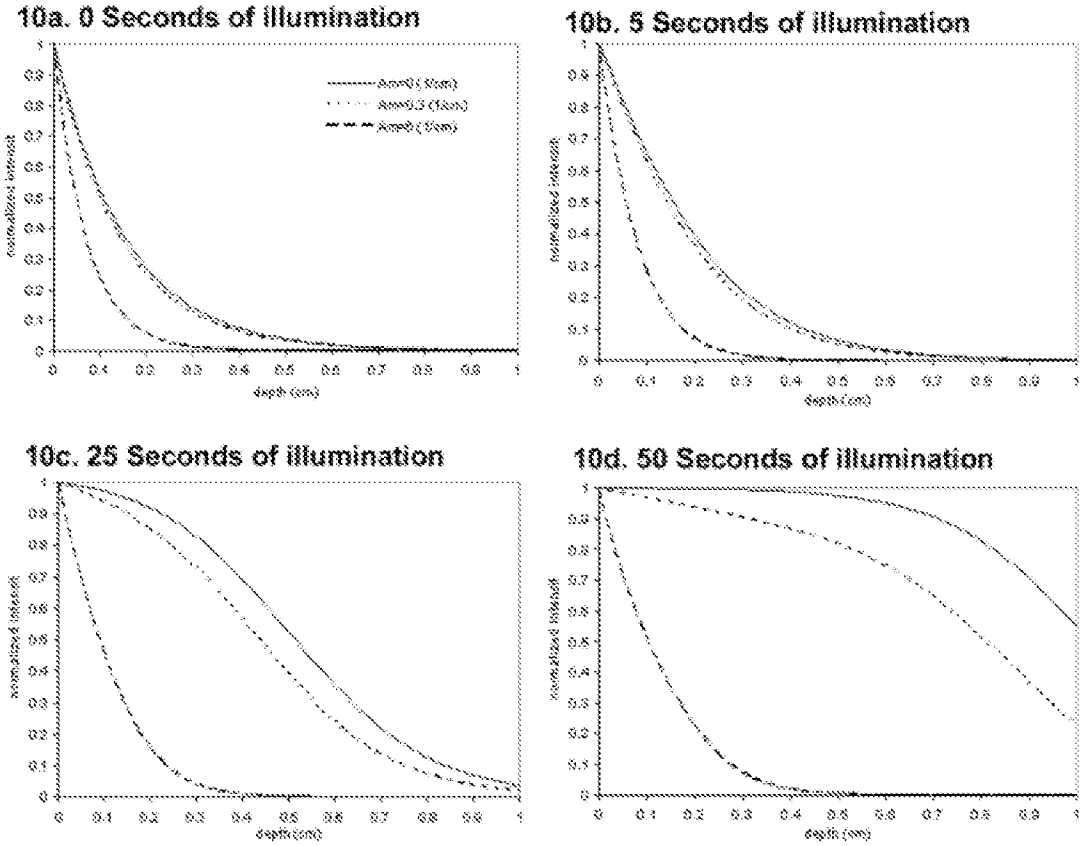

Figure 10. Effect of the monomer absorption coefficient on the intensity profile of a 1.0-cm sample. The light intensity is 10 mW/mm^2, C_0 is 0.0268 M (0.4 wt %), ϕ is 0.2, ϵ_i is 97.7 L (mol cm)$^{-1}$, and ϵ_p is 0 L (mol cm)$^{-1}$. Mesh sizes are 1.0 s and 0.025 cm.

ing exhibits an exponential decay in accordance with Beer's law, whereas the other two systems exhibit the sigmoidal shape characteristic of photobleaching systems. These results suggest that diffusion plays at most a moderate role in these photobleaching systems. In both Figures 12 and 13, the representative system with substantial diffusion lies much closer to the limiting system with no diffusion than to the limiting case of perfect mixing. Furthermore, in most photopolymerization systems, the operative diffusion coefficient is likely to be at least an order of magnitude smaller than the value of 0.001 cm^2/s that we chose for these studies. In addition, the diffusional mobility of the photoinitiator will be further restricted by the formation of the polymer matrix in these photopolymerization systems. On the basis of these studies, we expect diffusion to have negligible effects in most photobleaching systems because the diffusional timescale is large relative to that of photoinitiation. Diffusion will play the largest role in systems containing high photoinitiator concentrations and will tend to broaden the propagating photoinitiation front in these systems.

CONCLUSIONS

In this article, we have presented a description of the spatial and temporal evolution of the light intensity gradient, initiator concentration gradient, and initiation rate profiles for photobleaching initiator systems. This article builds on the foundation provided by researchers' previous contributions by generalizing the governing differential equations to include the effects of absorption by the initiator fragments, absorption by the monomer, and diffusion of the initiator. Because of the complexity of the resulting set of coupled differential equations, a numerical solution has been obtained with the method of finite differences. Simulation results have confirmed that, at any given time, the initiation rate profile resembles a wave front, and the breadth of this front is determined by factors such as the initial initiator concentration and the molar absorptivity.

The simulation results suggest that there is an optimum initiator concentration for the efficient photopolymerization of thick samples. For initiator concentrations above the optimum, the depth

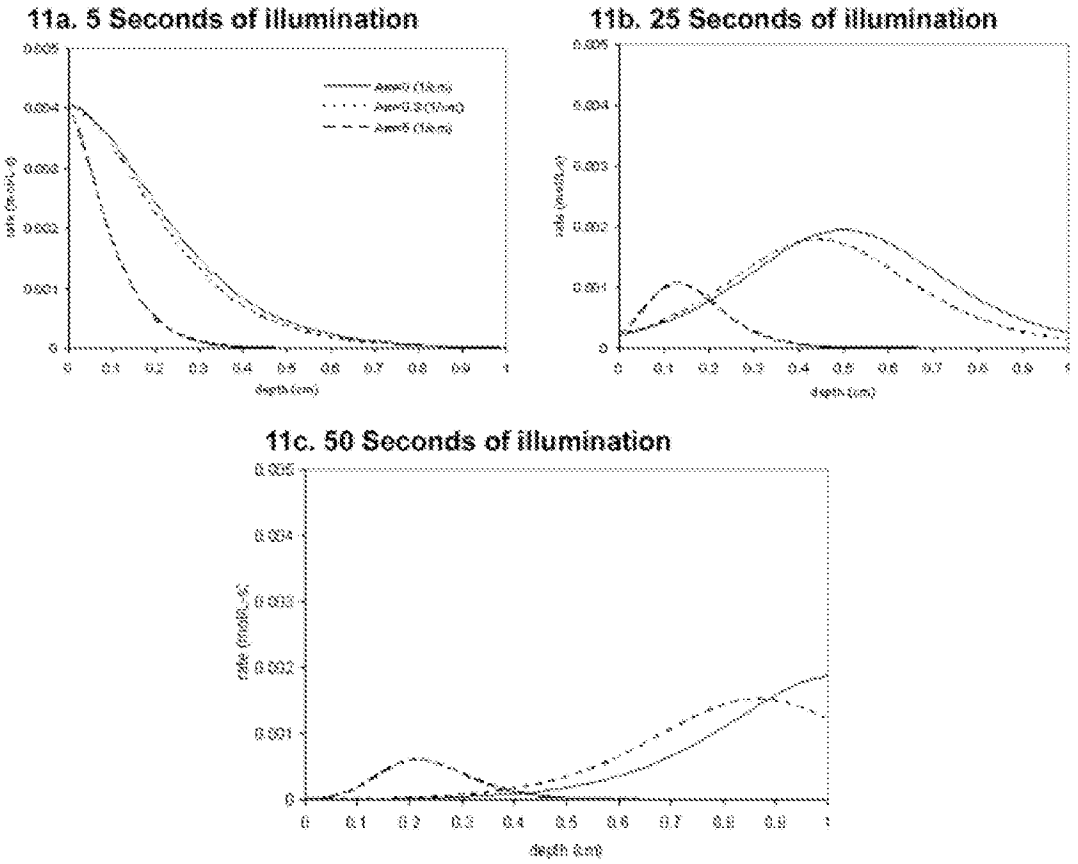

Figure 11. Effect of the monomer absorption coefficient on the photoinitiation rate of a 1.0-cm sample. The light intensity is 10 mW/mm^2, C_0 is 0.0268 M (0.4 wt %), ϕ is 0.2, ϵ_i is 97.7 L (mol cm)$^{-1}$, and ϵ_p is 0 L (mol cm)$^{-1}$. Mesh sizes are 1.0 s and 0.025 cm.

of light penetration and the spatial propagation of the photoinitiation front are restricted, whereas for concentrations below the optimum, the photoinitiation rate is limited by the lack of initiator. As the initiator concentration is increased, the initiation rate at the peak of the wave front is increased, although the rate of propagation of the front through the sample is decreased.

The initiator absorptivity has two competing effects on the photoinitiation effectiveness for deep cure. A low molar absorptivity allows more efficient penetration of light into the sample; however, a higher molar absorptivity leads to higher rates of photon absorption and higher rates of bleaching. In addition, as the initiator molar absorptivity increases, the maximum initiation rate increases, the breadth of the propagating front decreases, and the rate of spatial propagation through the sample decreases.

Simulation results have revealed that it is important to optimize the initiator concentration and absorptivity separately. For example, for two systems with the same optical density, the system with the higher initiator absorptivity will photobleach more rapidly, and the photoinitiation front will propagate more rapidly through the thickness of the sample. In contrast to the effects of the initial initiator concentration and absorptivity, an increase in the initiator quantum yield results in an increase in both the maximum photoinitiation rate and the rate of spatial propagation of the polymerization front.

The simulation results illustrate the importance of photobleaching for effective thick-section cure. As the molar absorptivity of the photolysis products is reduced, the rate of propagation of the photoinitiation front increases (the light intensity gradient and, therefore, the photoinitiation front are completely stagnant in the nonbleaching case). Under simulation conditions, the photoinitiation front can reach a depth of 1 cm in less than a minute. The simulation results have confirmed that the absorption of light by the monomer or polymer makes much less efficient use of the incident photons. Therefore, by selecting an initiation wavelength that the monomer does not ab-

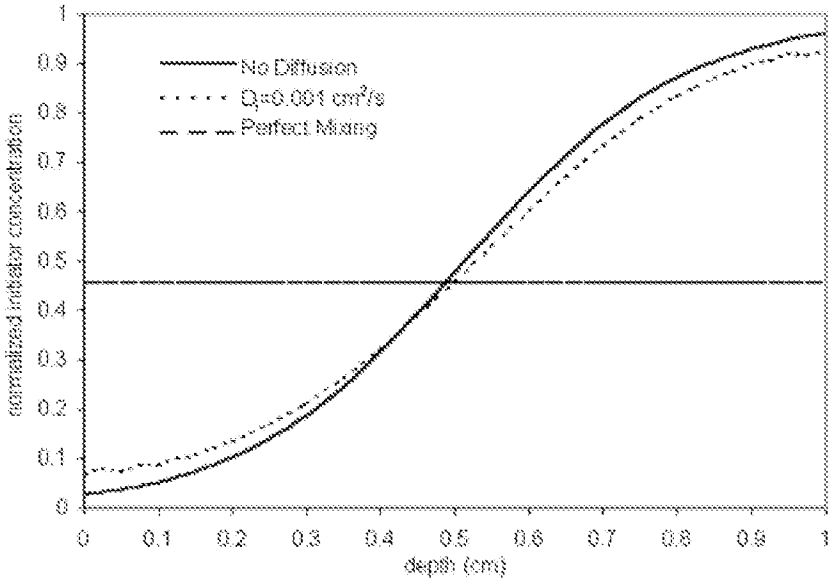

Figure 12. Effect of the initiator diffusion on the concentration profile of a 1.0-cm sample at 25 s. The light intensity is 10 mW/mm^2, C_0 is 0.0268 M (0.4 wt %), ϕ is 0.2, ϵ_i is 97.7 L (mol cm)$^{-1}$, and ϵ_p is 0 L (mol cm)$^{-1}$. Mesh sizes are 1.0 s and 0.025 cm.

sorb, we can significantly increase the maximum photoinitiation rate (indeed, it is possible to increase the photoinitiation rate throughout the sample) and increase the rate of spatial propagation of the polymerization front. Finally, on the basis of these studies, we expect diffusion to have negligible effects in most photobleaching systems because the diffusional timescale is large relative to that of photoinitiation. Diffusion will play the largest role in systems containing high photoinitiator concentrations and will tend to broaden the propagating photoinitiation front in these systems. This model provides a valuable tool for evaluating

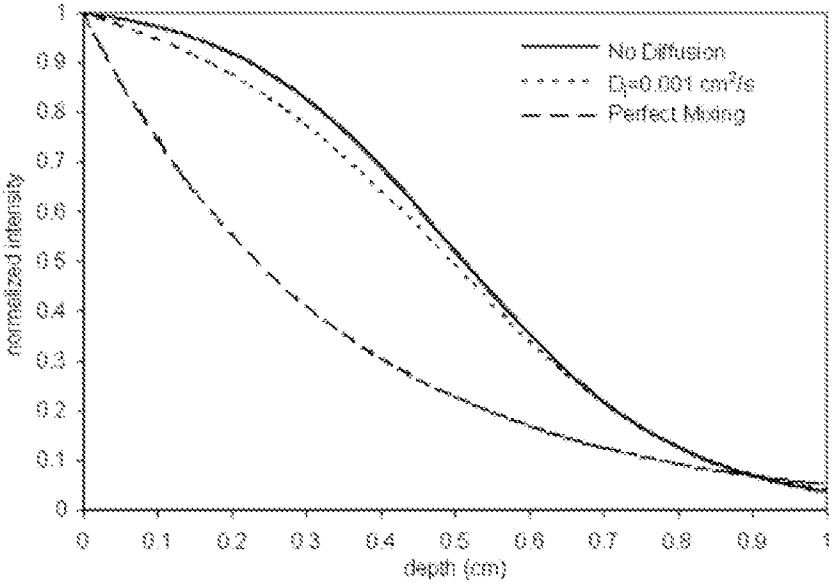

Figure 13. Effect of the initiator diffusion on the intensity profile of a 1.0-cm sample at 25 s. The light intensity is 10 mW/mm^2, C_0 is 0.0268 M (0.4 wt %), ϕ is 0.2, ϵ_i is 97.7 L (mol cm)$^{-1}$, and ϵ_p is 0 L (mol cm)$^{-1}$. Mesh sizes are 1.0 s and 0.025 cm.

the effectiveness of photobleaching initiator systems for thick-section cure.

This article is based on work supported by the Industry/University Cooperative Research Center for Fundamentals and Applications of Photopolymerization.

REFERENCES AND NOTES

1. Cramer, N. B.; Bowman, C. N. J Polym Sci Part A: Polym Chem 2001, 39, 3311–3319.
2. Padon, K. S.; Scranton, A. B. J Polym Sci Part A: Polym Chem 2001, 39, 715–723.
3. Padon, K. S.; Scranton, A. B. J Polym Sci Part A: Polym Chem 2000, 38, 3336–3346.
4. Crivello, J. V.; Dietliker, K. Photoinitiators for Free Radical and Cationic Photopolymerisation; Wiley: New York, 1998.
5. Fouassier, J. P. Photoinitiation Photopolymerization and Photocuring; Hanser: Cincinnati, OH, 1995.
6. Crivello, J. V.; Sangermano, M. J Polym Sci Part A: Polym Chem 2001, 39, 343–356.
7. Burdick, J. A.; Philpott, L. M.; Anseth, K. S. J Polym Sci Part A: Polym Chem 2001, 39, 683–692.
8. Kim, B. S.; Hrkach, J. S.; Langer, R. J Polym Sci Part A: Polym Chem 2000, 38, 1277–1282.
9. Stieger, E. M. M.; Klee, J. E.; Frey, H.; Mulhaupt, R. J Polym Sci Part A: Polym Chem 2001, 39, 4274–4282.
10. Narayanan, V.; Scranton, A. B. Trends Polym Sci 1997, 5, 415–419.
11. Baikerikar, K. K.; Scranton, A. B. Polymer 42, 2001, 431–441.
12. Baikerikar, K. K.; Scranton, A. B. J Appl Polym Sci 2001, 81, 3449–3461.
13. Coons, L. S.; Rangarajan, B.; Godshall, D.; Scranton, A. B. Am Chem Soc Symp Ser 1997, 673, 203–218.
14. Lewis, F. D.; Lauterbach, R. T.; Heine, H. G.; Harmann, W.; Rudolph, H. J Am Chem Soc 1975, 97, 1519–1525.
15. Finter, J.; Riediker, M.; Rohde, O.; Rotzinger, B. Makromol Chem Macromol Symp 1989, 24, 177–187.
16. Terrones, G.; Pearlstein, A. J. Macromolecules 2001, 34, 3195–3204.
17. Ivanov, V. V.; Decker, C. Polymer Int 2001, 50, 113–118.